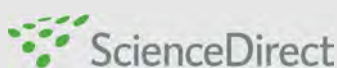
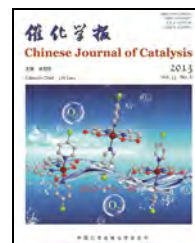


available at www.sciencedirect.com



journal homepage: www.elsevier.com/locate/chnjc

**Article****Effect of sulfur doping on the photocatalytic performance of BiVO₄ under visible light illumination**Zhenxuan Zhao^a, Hongxing Dai^{a,*}, Jiguang Deng^a, Yuxi Liu^a, Chak Tong Au^{b,#}^a Laboratory of Catalysis Chemistry and Nanoscience, Department of Chemistry and Chemical Engineering, College of Environmental and Energy Engineering, Beijing University of Technology, Beijing 100124, China^b Department of Chemistry and Center for Surface Analysis and Research, Hong Kong Baptist University, Kowloon Tong, Kowloon, Hong Kong, China**ARTICLE INFO****Article history:**

Received 11 March 2013

Accepted 5 June 2013

Published 20 August 2013

Keywords:

Sulfur doping

Bismuth vanadate

Visible-light-driven photocatalyst

Olive-like morphology

Methlyene blue degradation

Formaldehyde degradation

ABSTRACT

Porous monoclinic bismuth vanadate ($\text{BiVO}_{4-\delta}$) and sulfur-doped bismuth vanadates ($\text{BiVO}_{4-\delta}\text{S}_{0.08}$, $\text{BiVO}_{4-\delta}\text{S}_{0.09}$, and $\text{BiVO}_{4-\delta}\text{S}_{0.12}$) were synthesized by a dodecylamine-assisted alcohol-hydrothermal route in the absence and presence of thiourea or Na_2S . The physicochemical properties of the materials were characterized and their photocatalytic performance for the degradation of methylene blue and formaldehyde under visible light was evaluated. The samples have a single phase monoclinic scheelite crystal structure with a porous olive-like morphology, surface areas of 8.4–12.5 m^2/g , and bandgap energies of 2.40–2.48 eV. Surface Bi^{5+} , Bi^{3+} , V^{5+} , and V^{4+} species were present on the S-doped $\text{BiVO}_{4-\delta}$ samples. Sulfur doping influenced the surface $\text{Bi}^{5+}/\text{Bi}^{3+}$, $\text{V}^{5+}/\text{V}^{4+}$, and $\text{O}_{\text{ads}}/\text{O}_{\text{lat}}$ molar ratios, and the amount of sulfur doped had an important effect on the photocatalytic performance. Under visible light, $\text{BiVO}_{4-\delta}\text{S}_{0.08}$ performed the best in the photodegradation of methylene blue and formaldehyde. A higher surface oxygen species concentration and a lower bandgap energy were responsible for the excellent visible light photocatalytic performance of $\text{BiVO}_{4-\delta}\text{S}_{0.08}$.

© 2013, Dalian Institute of Chemical Physics, Chinese Academy of Sciences.

Published by Elsevier B.V. All rights reserved.

1. Introduction

Photocatalytic technology is one of the most effective pollution control method. Various kinds of effective and low cost photocatalysts for the degradation of organic pollutants have been investigated. TiO_2 has a large bandgap energy (≥ 3.2 eV) and it is only active under UV light, which is only 4% of the solar energy. In recent years, considerable attention has been paid to the synthesis of visible light-responsive photocatalysts. A number of heteroatoms (N, C, S, or F) and metals (La, Fe, or Cr) were used to dope TiO_2 to make its bandgap energy narrower (to 2.5–3.0 eV). Meanwhile, Ti-free mixed oxide photo-

catalysts, such as Bi_3NbO_7 [1] and $\text{Bi}_2\text{W}_2\text{O}_9$ [2], with bandgap energies of 2.0–3.8 eV were reported to have high photocatalytic activity for the degradation of organic materials under visible light illumination. BiVO_4 is an effective photocatalyst for the splitting of water [3] and the oxidative degradation of rhodamine B (RhB) [4], methyl orange [5], methylene blue (MB) [6], copper acetylacetone [7,8], 4-alkylphenols [9], and phenol [5].

It is well known that the catalytic performance of a photocatalyst is related to its surface area, crystal structure, oxygen deficiency, pore structure, crystallite size, and particle morphology. Monoclinic scheelite BiVO_4 exhibits a higher photo-

^{*} Corresponding author. Tel: +86-10-6739-6118; Fax: +86-10-6739-1983; E-mail: hxdai@bjut.edu.cn[#] Corresponding author. Tel: +852-3411-7067; Fax: +852-3411-7348; E-mail: pctau@hkbu.edu.hk

The work was supported by the National Natural Science Foundation of China (21077007), the Discipline and Postgraduate Education Foundation (005000541212014), the Funding Project for Academic Human Resources Development in Institutions of Higher Learning under the Jurisdiction of Beijing Municipality (PHR201107104), and Hong Kong Baptist University Foundation (FRG2/09-10/023).

DOI: 10.1016/S1872-2067(12)60632-9 | http://www.sciencedirect.com/science/journal/18722067 | Chin. J. Catal., Vol. 34, No. 8, August 2013

catalytic activity than its tetragonal zircon and tetragonal scheelite counterparts [10,11], which is because it has a lower bandgap energy (2.4 eV) than they do (2.9–3.1 eV). Hierarchical BiVO₄/Bi₂O₂CO₃ nanocomposites have shown good photocatalytic performance in the degradation of RhB due to their unique two-dimensional sheet-like morphology, large surface area, and high crystallinity [12]. The doping of a small amount of a heteroatom X (X = F, N, S) into the lattice of a parent metal oxide can result in the narrowing of the band gap by the hybridization of the X 2p and O 2p orbitals, thus enhancing the absorption of visible light [13]. Furthermore, the generation of oxygen vacancies from X doping can also enhance photocatalytic activity. For example, the formation of oxygen vacancies in TiO₂ induced by F- and N-doping is the main factor for the enhancement in visible light-responsive catalytic activity [14]. The doping of F⁻ into the SrTiO₃ lattice narrows its band gap and generates Ti³⁺ and oxygen vacancies, hence promoting electron mobility [15].

Many groups have reported the synthesis and photocatalytic applications of S-doped photocatalysts. For example, S-doped TiO₂ exhibited a much higher activity than the N-doped and undoped counterparts [16]. Long et al. [17] found that the S 3p orbital is located above the top of the valence band (VB) and it is mixed with the O 2p state, thus decreasing the bandgap energy. During their investigation of a S-doped ZnO photocatalyst, Shen et al. [18] observed that the intensity of the UV emission peak decreased with increased S concentration. Li et al. [14] reported that S-doped In(OH)₃ was responsive to visible light for the degradation of acetone and dyes. However, there have no reports on the synthesis and photocatalytic applications of S-doped BiVO₄ in the literature.

Previously, our group reported the synthesis and physicochemical property characterization of porous and morphological diverse monoclinic BiVO₄ samples, such as a porous octapod-like monoclinic BiVO₄ for the removal of phenol and MB [19], a porous spherical BiVO₄ for the degradation of methyl orange [20], polyhedral, rod-like, leaf-like, and spherical BiVO₄ for the degradation of MB [21], three-dimensionally ordered macroporous BiVO₄ for the degradation of phenol [22], and flower-, sheet-, and rod-like and spherical BiVO₄ for the degradation of methyl orange [23]. In this paper, we report the synthesis and photocatalytic activity of S-doped BiVO₄ with a porous olive-like morphology for the degradation of MB and formaldehyde under visible light illumination.

2. Experimental

2.1. Catalyst preparation

Porous olive-like BiVO₄ was prepared by the dodecylamine (DA)-assisted alcohol-hydrothermal method [5] using Bi(NO₃)₃·5H₂O and NH₄VO₃ as metal source, DA as surfactant, and ethanol and ethylene glycol (EG) as solvent. Concentrated nitric acid (5 ml) and DA (30 mmol) were added to 25 ml of ethanol and EG (volumetric ratio = 1:1) mixed solution. Bi(NO₃)₃·5H₂O (10 mmol) and NH₄VO₃ (10 mmol) were dissolved in the mixed solution. The pH value was adjusted to 1.5

using NaOH aqueous solution containing absolute ethanol and EG (volumetric ratio = 1:1). The mixture (80 ml) was transferred into a Teflon-lined stainless steel autoclave for alcohol-hydrothermal treatment at 100 °C for 12 h. After washing with deionized water and ethanol and drying at 80 °C overnight, the solid was calcined in air using a ramp of 1 °C/min from room temperature (RT) to 450 °C and kept at this temperature for 4 h, thus obtaining the BiVO₄ sample.

The S-doped BiVO₄ photocatalysts were synthesized using three methods. One was the DA-assisted alcohol-hydrothermal method. The procedure was the same as for BiVO_{4-δ} preparation, except that the pH value was adjusted to 1.5 using Na₂S solution containing absolute ethanol and EG (ethanol/EG volumetric ratio = 1:1). The second method was to use uncalcined olive-like BiVO₄ soaked in a thiourea aqueous solution (BiVO₄/thiourea molar ratio = 1:2) under stirring and then dried at RT. The material obtained was calcined using a ramp of 1 °C/min in a muffle furnace at 300 °C for 2 h and 450 °C for 3 h. The third method was the same as that of the second one, except that the BiVO₄/thiourea molar ratio was 1:4. Inductively coupled plasma atomic emission spectroscopic (ICP-AES) analysis indicated that the S content was 1.17, 0.49, and 0.78 wt% for the S-doped BiVO₄ samples with Na₂S and thiourea (BiVO₄/thiourea molar ratios of 1:2 and 1:4) as sulfur source, respectively, i.e., the samples were BiVO_{4-δ}S_{0.12}, BiVO_{4-δ}S_{0.05}, and BiVO_{4-δ}S_{0.08}, respectively.

All chemicals (AR) were purchased from Beijing Chemicals Company and used without further purification.

2.2. Catalyst characterization

X-ray diffraction (XRD) patterns of the BiVO₄ and S-doped BiVO₄ catalysts were recorded on a Bruker/AXS D8 Advance X-ray diffractometer operated at 40 kV and 35 mA with a Cu K_α X-ray irradiation source ($\lambda = 0.15406$ nm). The surface areas were determined by N₂ adsorption at -196 °C on a Micromeritics ASAP 2020 adsorption analyzer. Before measurement, the catalyst was degassed at 250 °C for 3 h. The surface area was calculated using the Brunauer-Emmett-Teller (BET) method. Scanning electron microscopy (SEM) was conducted on a Gemini Zeiss Supra 55 apparatus operated at 10 kV. Transmission electron microscope (TEM) images of typical samples were obtained using a JEOL JEM-2010 instrument. X-ray photoelectron spectroscopy (XPS) was used to determine the Bi 4f, V 2p, O 1s, and S 1s binding energies (BEs) of surface bismuth, vanadium, oxygen, and sulfur species, respectively, with Mg K_α ($h\nu = 1253.6$ eV) as the excitation source. Before the XPS measurement, the catalyst was pretreated in an O₂ flow of 20 ml/min at 450 °C for 1 h. After cooling to room temperature, the catalyst was transferred to a holder in a Glove Bag (Instruments for Research and Industry, USA) that was filled with He, and then the holder was transferred into the spectrometer chamber under He. Before being analyzed in the analysis chamber, the pretreated catalyst was outgassed in the preparation chamber for 0.5 h. The C 1s signal at BE = 284.6 eV was taken as a reference for BE calibration. The chemical composition of the samples was analyzed using X-ray fluorescence

spectroscopy (XRF, Magix PW2403, PANalytical) with a ceramic X-ray tube operated at 3 kW. The sample was finely ground, then placed on a polyethylene plate and compressed into a wafer with a diameter of 3 cm and a thickness of 2–5 mm. The ultraviolet-visible (UV-Vis) diffuse reflectance spectra of the catalysts in the range of 200–800 nm were measured on a Shimadzu UV-2450 UV-Vis spectrophotometer using BaSO₄ as the standard.

2.3. Photocatalytic evaluation

The oxidative degradation of MB and formaldehyde were adopted for the evaluation of the photocatalytic activity of the S-doped BiVO₄ samples in a quartz reactor under visible light irradiation using a 300-W Xe lamp with a 400 nm cutoff filter (Q0250, Beijing Changtuo Sci. & Technol. Co., Ltd.). The photocatalytic evaluation was conducted at RT as follows. The sample (0.01 g) was suspended in 100 ml of MB-containing aqueous solution (initial MB concentration $C_0 = 0.005, 0.01, 0.02, 0.03$ or 0.04 mmol/L). The sample (0.1 g) was added to 100 ml of a formaldehyde solution (initial formaldehyde concentration $C_0 = 0.04\%$). Before illumination, the solution was ultrasonically treated for 10 min and magnetically stirred for 2 h in the dark to ensure adsorption-desorption equilibrium. Then, the suspension was magnetically stirred and exposed to visible light illumination. The temperature of the reaction solution was kept at 25 °C using flowing cool water. The suspension (4 ml) was taken out at 30 min intervals and centrifuged to remove the photocatalyst particles for the analysis of the MB or formaldehyde concentration. The concentration (C_t) of MB or formaldehyde in the solution after time (t) was monitored by UV-Vis (UV-2010, Shimadzu) and GC (GC-2010, Shimadzu) equipment, respectively. The absorbance of the MB solution at 664 nm during the photodegradation process was determined with the UV-Vis apparatus. C_t/C_0 as well as the irradiation times $t_{1/2}$ and $t_{1/10}$ (corresponding to the irradiation time when MB conversion $C_t = (1/2)C_0$ and $(1/10)C_0$, where C_0 and C_t are the initial MB concentration and the MB concentration at a given reaction time (t), respectively) were used to evaluate the photocatalytic activity of the samples.

3. Results and discussion

3.1. Crystal phase composition

Figure 1 shows the XRD patterns of the BiVO_{4-δ} and S-doped BiVO_{4-δ} samples. All of the diffraction peaks could be indexed to the pure monoclinic scheelite BiVO₄ phase (space group: I2/a, JCPDS 14-0688) without any impurity phases such as the Na₂S, Bi₂S₃, or Na₂SO₃ phases. The results demonstrated that S²⁻ was homogeneously incorporated into the BiVO₄ lattice. Similar XRD patterns of BiVO₄ have also been recorded by our group [5] and other researchers [11,24,25]. Some discrepancies in the diffraction intensities of the samples were due to the different preparation procedures adopted. The calcination temperature (450 °C) was appropriate for the complete removal of the surfactant molecules.

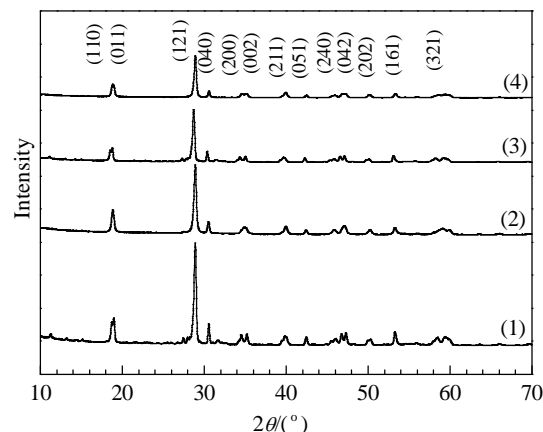


Fig. 1. XRD patterns of BiVO_{4-δ} (1), BiVO_{4-δS0.05} (2), BiVO_{4-δS0.08} (3), and BiVO_{4-δS0.12} (4).

3.2. Morphology, surface area, and pore size distribution

Representative SEM and TEM images of the BiVO_{4-δ} and S-doped BiVO_{4-δ} samples are shown in Fig. 2. The BiVO_{4-δ} sample displayed a regular olive-like morphology (Fig. 2(a) and (b)) with particle sizes of 1.1–3.0 μm. Macropores (diameter = 82–245 nm) were distributed randomly on the surface similar to those on a porous olive-like BiVO₄ [5]. The BiVO_{4-δS0.12} sample exhibited a uniform porous olive-like morphology (Fig. 2(j)–(l)) with particle sizes of 0.4–3.0 μm, indicating that the doping of S into the BiVO_{4-δ} lattice did not influence the particle morphology. The BiVO_{4-δS0.05} and BiVO_{4-δS0.08} samples were mainly composed of uniform porous olive-like microparticles with particle sizes of 0.5–5.2 μm (Fig. 2(d)–(f) and (g)–(i)), with a small number of particles of irregular morphology. From the high resolution TEM images (Fig. 2(c)) of the BiVO_{4-δ} sample, one can see that the lattice spacing (d value) of the (121) plane was 0.308 nm, which is close to that (0.31 nm) of the standard monoclinic BiVO₄ sample (JCPDS 14-0688). The S-doped BiVO_{4-δ} samples exhibited two kinds of lattice fringes of the (121) and (040) planes, with d values that were 0.309–0.310 and 0.292–0.293 nm, respectively, which are not much different from those of the standard monoclinic BiVO₄ sample.

Figure 3 shows the N₂ adsorption isotherms and pore size distribution of the samples. Their BET surface areas are summarized in Table 1. It is observed from Fig. 3(a) that the N₂ adsorption-desorption isotherms of these four samples indicated a combination of macroporous and mesoporous structures. The BiVO_{4-δ} sample exhibited a type II isotherm, while the BiVO_{4-δS0.05}, BiVO_{4-δS0.08}, and BiVO_{4-δS0.12} samples displayed a type III isotherm. The absence of an adsorption plateau at relative pressures near unity suggested the presence of macropores [26] from the aggregation of nano- or microparticles. The pore size distribution (Fig. 3(b)) of the samples showed one small peak in the range of 2.5–4.5 nm and one broad peak in the range of 10–100 nm, indicating the presence of mesopores and macropores in the samples, which confirmed the TEM observations (Fig. 2(b), (e), (h), and (k)). As can be seen in Table 1, the surface area of the BiVO_{4-δ} sample was 12.5

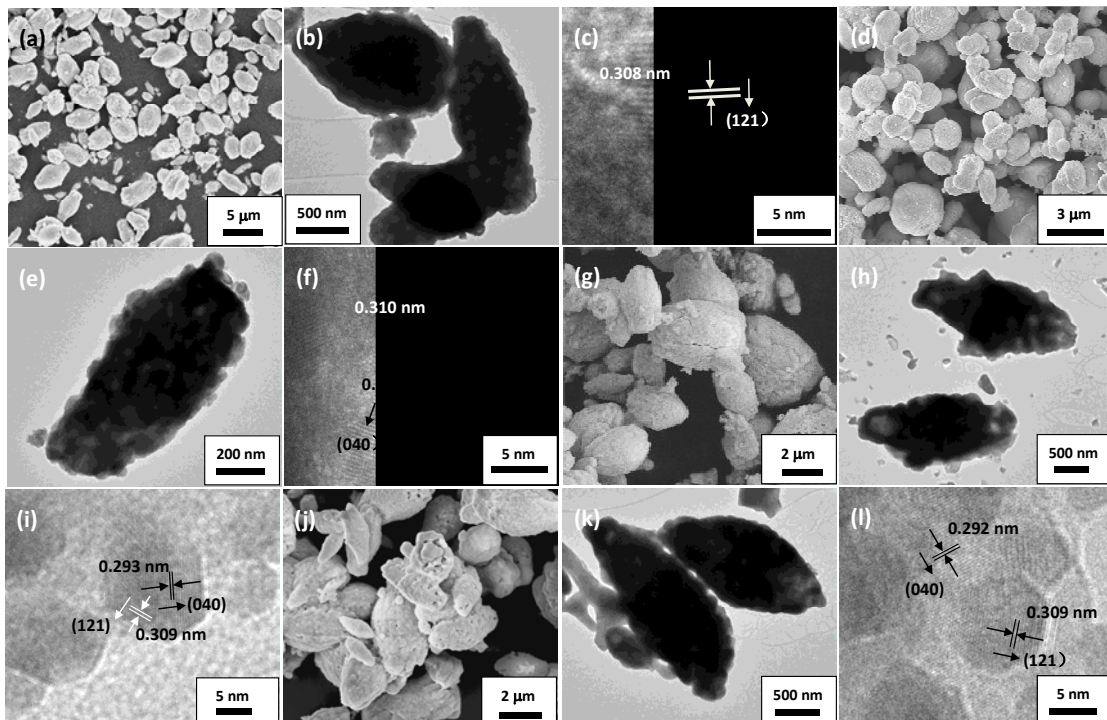


Fig. 2. SEM (a, d, g, and j) and TEM (b, c, e, f, h, i, k, and l) images of $\text{BiVO}_{4-\delta}$ (a–c), $\text{BiVO}_{4-\delta}\text{S}_{0.05}$ (d–f), $\text{BiVO}_{4-\delta}\text{S}_{0.08}$ (g–i), and $\text{BiVO}_{4-\delta}\text{S}_{0.12}$ (j–l).

m^2/g , which is similar to that of the porous olive-like BiVO_4 sample previously reported [5]. The surface areas of the S-doped $\text{BiVO}_{4-\delta}$ samples were in the range of 8.4–9.9 m^2/g , which were lower than that of the undoped sample.

3.3. Surface composition, metal oxidation state, and oxygen species

The surface composition, metal chemical state, and adsorbed species on the samples were characterized by XPS. Figure 4(a) shows the $\text{Bi } 4f$ XPS spectra of the samples. Two sets of $\text{Bi } 4f$ spin-orbit doublet components, $\text{Bi } 4f_{5/2}$ and $\text{Bi } 4f_{7/2}$, together with the typical $\text{Bi } 4f$ spin-orbit splitting of 5.3 eV [27,28], were recorded. For the $\text{BiVO}_{4-\delta}$ sample, there were two symmetrical peaks at 158.7 and 164.0 eV, which were assigned to the $\text{Bi } 4f_{7/2}$ and $\text{Bi } 4f_{5/2}$ signals of surface Bi^{3+} species [29–31], respectively. The $\text{Bi } 4f$ spectra of the three S-doped $\text{BiVO}_{4-\delta}$ samples could be decomposed into four components at 158.7, 159.8, 164.0, and 165.1 eV. The components at 158.7 and 164.0 eV were attributed to surface Bi^{3+} species, while the ones at 159.8 and 165.1 eV were assigned to surface Bi^{5+} species [32,33]. This showed that there were surface Bi^{3+} species on $\text{BiVO}_{4-\delta}$ and surface Bi^{3+} and Bi^{5+} species on $\text{BiVO}_{4-\delta}\text{S}_{0.05}$, $\text{BiVO}_{4-\delta}\text{S}_{0.08}$, and $\text{BiVO}_{4-\delta}\text{S}_{0.12}$. The result indicated that the doping of S^{2-} into the $\text{BiVO}_{4-\delta}$ lattice induced a change in the Bi oxida-

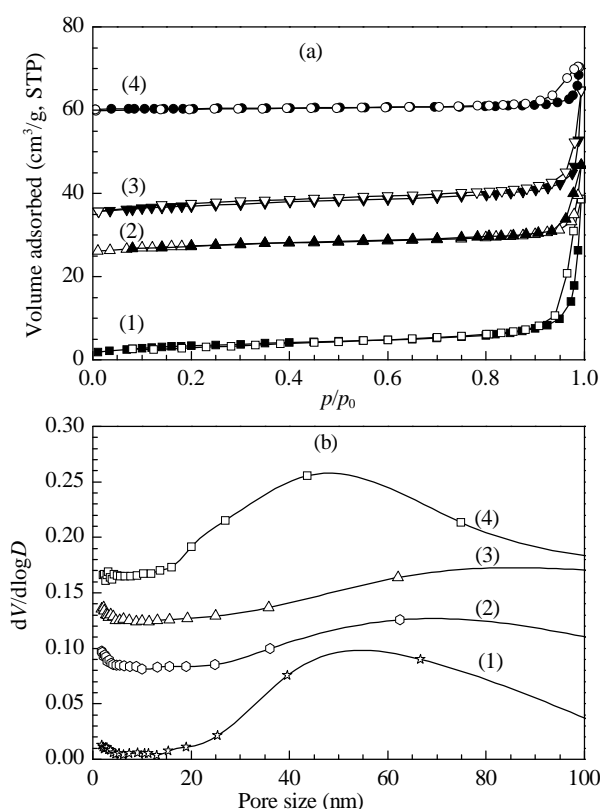


Fig. 3. N_2 adsorption isotherms (a) and pore size distribution (b) of $\text{BiVO}_{4-\delta}$ (1), $\text{BiVO}_{4-\delta}\text{S}_{0.05}$ (2), $\text{BiVO}_{4-\delta}\text{S}_{0.08}$ (3), and $\text{BiVO}_{4-\delta}\text{S}_{0.12}$ (4).

Table 1

Preparation parameters, crystal phase, BET surface area (A_{BET}), and bandgap energy of the $\text{BiVO}_{4-\delta}$ and S-doped $\text{BiVO}_{4-\delta}$ photocatalysts.

Photocatalyst	Sulfur source	Crystal phase	A_{BET} (m^2/g)	Bandgap energy (eV)
$\text{BiVO}_{4-\delta}$	–	monoclinic	12.5	2.48
$\text{BiVO}_{4-\delta}\text{S}_{0.05}$	(BiVO_4 /thiourea molar ratio = 1:2)	monoclinic	8.4	2.41
$\text{BiVO}_{4-\delta}\text{S}_{0.08}$	(BiVO_4 /thiourea molar ratio = 1:4)	monoclinic	9.9	2.40
$\text{BiVO}_{4-\delta}\text{S}_{0.12}$	Na_2S	monoclinic	9.4	2.43

tion state distribution. This effect has also been observed with F- or Cl-doped $\text{Bi}_2\text{Sr}_2\text{CaCu}_2\text{O}_8$ [32]. Figure 4(b) shows the V $2p_{3/2}$ XPS spectra of the samples. The asymmetrical V $2p_{3/2}$ signal could be decomposed into two components at 515.9 and 517.6 eV, assigned to surface V^{4+} and V^{5+} species [34–36], respectively. By the electroneutrality principle, we deduced that all of the samples were oxygen-deficient (i.e., $\text{BiVO}_{4-\delta}$ or $\text{BiVO}_{4-\delta}\text{S}_\sigma$) and the surface nonstoichiometric oxygen amount (δ) depended upon the surface $\text{V}^{5+}/\text{V}^{4+}$ and/or $\text{Bi}^{5+}/\text{Bi}^{3+}$ molar ratios. This is summarized in Table 2.

In the O 1s XPS spectra of the samples (Fig. 4(c)), the asymmetrical O 1s spectrum could be decomposed into two components at 529.8 and 532.0 eV, which were attributed to surface lattice oxygen (O_{latt}) and surface adsorbed oxygen (O_{ads}) species [37,38], respectively. The presence of species such as OH^- , CO_3^{2-} , and physically adsorbed H_2O on the surface was minimized by the pretreatment of the samples before the XPS measurements. Because the BEs of the S 2p signals are between

161 and 162 eV [39,40], which overlapped the BEs (156–167 eV) of the Bi 4f spin-orbit doublet components, we recorded the S 1s spectra of the samples, as shown in Fig. 4(d). For the three S-doped $\text{BiVO}_{4-\delta}$ samples, there was only one S 1s signal at 233 eV assigned to surface S^{2-} species. This result indicated that sulfur was successfully incorporated into the $\text{BiVO}_{4-\delta}$ lattice. In addition, the signal intensity increased in the sequence of $\text{BiVO}_{4-\delta}\text{S}_{0.05} < \text{BiVO}_{4-\delta}\text{S}_{0.08} < \text{BiVO}_{4-\delta}\text{S}_{0.12}$, implying that more S^{2-} was doped into the $\text{BiVO}_{4-\delta}$ lattice than into the $\text{BiVO}_{4-\delta}\text{S}_{0.12}$ sample.

The surface and bulk compositions of the samples estimated by the quantitative analysis of the XPS and XRF spectra are summarized in Table 2. There was surface Bi enrichment on the $\text{BiVO}_{4-\delta}$ and S-doped samples. The surface $\text{Bi}^{5+}/\text{Bi}^{3+}$ and $\text{O}_{\text{ads}}/\text{O}_{\text{latt}}$ molar ratios increased in the sequence of $\text{BiVO}_{4-\delta} < \text{BiVO}_{4-\delta}\text{S}_{0.05} < \text{BiVO}_{4-\delta}\text{S}_{0.08} < \text{BiVO}_{4-\delta}\text{S}_{0.12}$. The $\text{BiVO}_{4-\delta}\text{S}_{0.08}$ sample possessed the highest surface $\text{Bi}^{5+}/\text{Bi}^{3+}$ (0.26) and $\text{O}_{\text{ads}}/\text{O}_{\text{latt}}$ (2.85) molar ratios. The bulk Bi/V molar ratios were close to

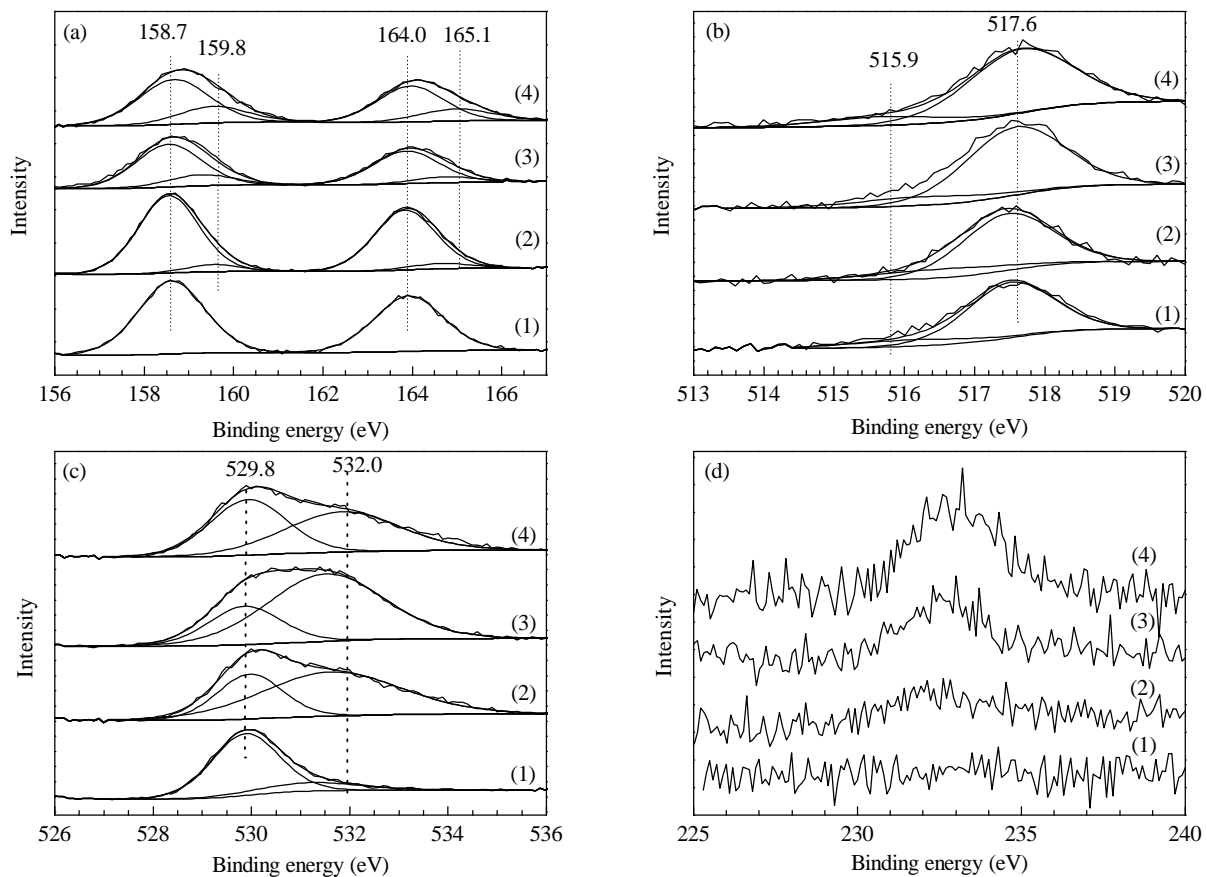


Fig. 4. Bi 4f(a), V $2p_{3/2}$ (b), O 1s (c), and S 1s (d) XPS spectra of $\text{BiVO}_{4-\delta}$ (1), $\text{BiVO}_{4-\delta}\text{S}_{0.05}$ (2), $\text{BiVO}_{4-\delta}\text{S}_{0.08}$ (3), and $\text{BiVO}_{4-\delta}\text{S}_{0.12}$ (4).

Table 2

Surface and bulk compositions of the $\text{BiVO}_{4-\delta}$ and S-doped $\text{BiVO}_{4-\delta}$ photocatalysts.

Photocatalyst	Surface composition ^a (molar ratio)					Bulk composition ^b (molar ratio)	
	$\text{Bi}^{5+}/\text{Bi}^{3+}$	Bi/V	$\text{V}^{5+}/\text{V}^{4+}$	$\text{O}_{\text{ads}}/\text{O}_{\text{latt}}$	S/($\text{O}_{\text{ads}}+\text{O}_{\text{latt}}$)	Bi/V	S/O
$\text{BiVO}_{4-\delta}$	0	2.94	0.16	0.21	0	1.01	0
$\text{BiVO}_{4-\delta}\text{S}_{0.05}$	0.08	2.27	0.22	1.96	0.010	1.01	0.011
$\text{BiVO}_{4-\delta}\text{S}_{0.08}$	0.26	2.38	0.16	2.85	0.016	1.01	0.019
$\text{BiVO}_{4-\delta}\text{S}_{0.12}$	0.20	2.12	0.15	1.08	0.030	1.02	0.029

^aData obtained by XPS; ^bData obtained by XRF.

1.00, indicating that the $\text{BiVO}_{4-\delta}$ and S-doped $\text{BiVO}_{4-\delta}$ samples were stoichiometric. The surface $S/(O_{\text{ads}}+O_{\text{latt}})$ molar ratios of the samples were basically similar to their bulk ratios.

3.4. Optical absorption behavior

UV-Vis diffuse reflectance spectroscopy was used to characterize the optical absorption behavior of the samples. Figure 5(a) and (b) show the UV-Vis absorption spectra and optical absorption edges of the $\text{BiVO}_{4-\delta}$ and S-doped $\text{BiVO}_{4-\delta}$ samples. The samples exhibited strong absorption in the UV and visible light regions, which is a characteristic absorption feature of monoclinic BiVO_4 [41,42]. The steep shape of the spectra indicated that the visible light adsorption was due to the bandgap transition from the Bi 6s valence band (VB) to V 3d one [42,43]. We use the formula of $(\alpha h\nu)^2 = A(h\nu - E_g)^n$ to describe the relationship between the absorption coefficient (α) and incident photon energy ($h\nu$) [44,45], where A and E_g are a constant and the bandgap energy, respectively. The value of n is 1, which is characteristic of monoclinic BiVO_4 [5,46]. The bandgap energies of the $\text{BiVO}_{4-\delta}S_{0.05}$, $\text{BiVO}_{4-\delta}S_{0.08}$, and $\text{BiVO}_{4-\delta}S_{0.12}$ samples were in the range of 2.40–2.43 eV, which were narrower than that (2.48 eV) of the $\text{BiVO}_{4-\delta}$ sample. The light absorption ability of the S-doped $\text{BiVO}_{4-\delta}$ samples decreased with increased S-doped amount (Fig. 5(a)), in the order of $\text{BiVO}_{4-\delta}S_{0.08} < \text{BiVO}_{4-\delta}S_{0.05} < \text{BiVO}_{4-\delta}S_{0.12} < \text{BiVO}_{4-\delta}$ while the bandgap energy

(Fig. 5(b)) became narrower in the same sequence. Hussain et al. [47] also observed that the bandgap energy was reduced with increasing S-doping level. Yang et al. [48] suggested that the S impurity decreased the bandgap energy by the mixing of the Bi 6s VB with S 3p. In addition, the mixing states of S 3s and O 2p located in the band gap can result in a reduced photon absorption energy. These results clearly demonstrated that the amount of doped S influenced the light absorbing ability and the bandgap energy.

3.5. Photocatalytic degradation of MB

The photocatalytic activity of the samples was evaluated for the degradation of MB and formaldehyde in aqueous solution under visible light illumination. Figure 6(a) presents the photocatalytic performance of the samples. The $t_{1/2}$ and $t_{1/10}$ values are summarized in Table 3. An ultrasonic treatment and stirring process in the dark were adopted to establish adsorption-desorption equilibrium. The MB conversion increased with irradiation time, and the S-doped $\text{BiVO}_{4-\delta}$ samples showed a catalytic activity ($t_{1/10} = 136$ –207 min) much higher than that ($t_{1/10} = 239$ min) of the $\text{BiVO}_{4-\delta}$ sample. The $\text{BiVO}_{4-\delta}S_{0.08}$ sample performed the best ($t_{1/10} = 136$ min). Clearly, the photocatalytic performance of the sample improved after sulfur doping. A similar phenomenon was also observed in both phenol degradation and $\text{CO}_2 + \text{H}_2\text{O}$ conversion over sulfur-doped TiO_2 pho-

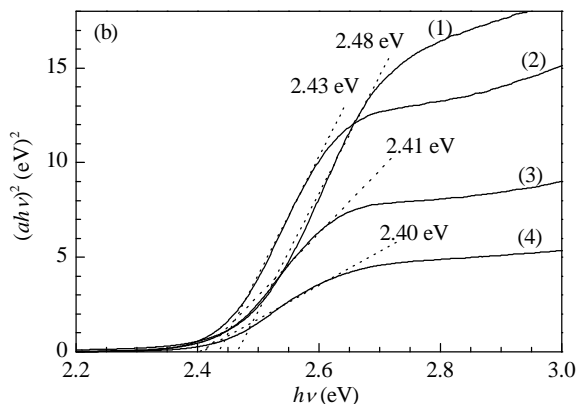
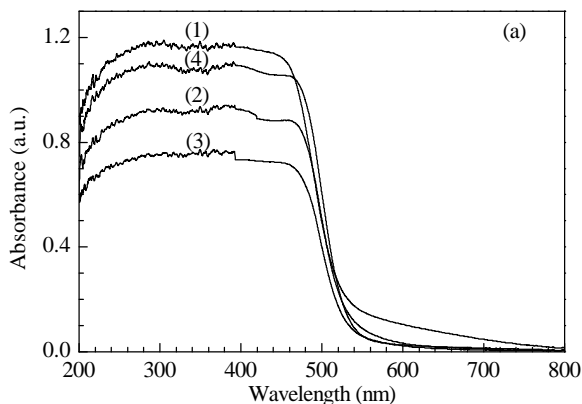


Fig. 5. UV-Vis diffuse reflectance spectra (a) and plots of the $(\alpha h\nu)^2$ versus $h\nu$ (b) of $\text{BiVO}_{4-\delta}$ (1), $\text{BiVO}_{4-\delta}S_{0.05}$ (2), $\text{BiVO}_{4-\delta}S_{0.08}$ (3), and $\text{BiVO}_{4-\delta}S_{0.12}$ (4).

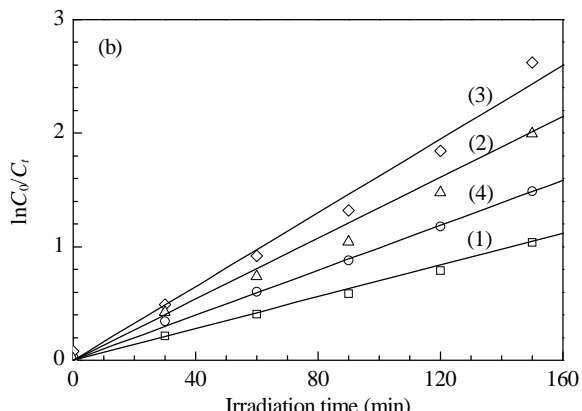
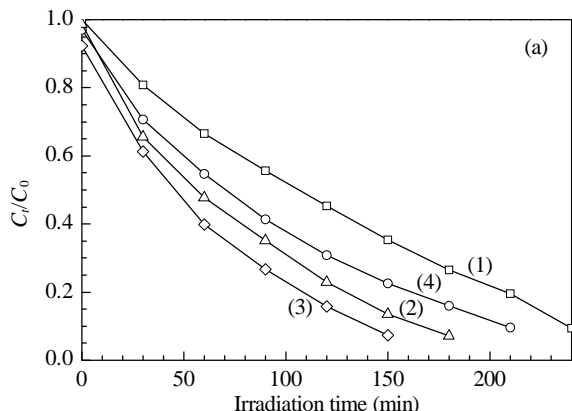


Fig. 6. Degradation of MB over 0.01 g of $\text{BiVO}_{4-\delta}$ (1), $\text{BiVO}_{4-\delta}S_{0.05}$ (2), $\text{BiVO}_{4-\delta}S_{0.08}$ (3), and $\text{BiVO}_{4-\delta}S_{0.12}$ (4) under visible light ($\lambda \geq 400$ nm) illumination. Reaction conditions: $C_0 = 0.01$ mmol/L, temperature = 25 °C, MB solution volume = 100 ml.

Table 3

Correlation coefficients (R^2), rate constants (k), $t_{1/2}$, and $t_{1/10}$ values of the $\text{BiVO}_{4-\delta}$ and S-doped $\text{BiVO}_{4-\delta}$ photocatalysts for MB degradation.

Photocatalyst	$C_0/\text{mmol/L}$	R^2	k/min^{-1}	$t_{1/2}/\text{min}$	$t_{1/10}/\text{min}$
$\text{BiVO}_{4-\delta}$	0.01	0.997	0.0068	105	239
$\text{BiVO}_{4-\delta}\text{S}_{0.05}$	0.01	0.991	0.0128	56	165
$\text{BiVO}_{4-\delta}\text{S}_{0.08}$	0.01	0.983	0.0164	45	136
$\text{BiVO}_{4-\delta}\text{S}_{0.12}$	0.01	0.999	0.0096	71	207
$\text{BiVO}_{4-\delta}\text{S}_{0.08}$	0.005	0.973	0.0226	30	105
$\text{BiVO}_{4-\delta}\text{S}_{0.08}$	0.02	0.991	0.0079	105	260
$\text{BiVO}_{4-\delta}\text{S}_{0.08}$	0.03	0.994	0.0052	136	315
$\text{BiVO}_{4-\delta}\text{S}_{0.08}$	0.04	0.994	0.0041	178	375

tocatalysts under UV and solar irradiation [47,49].

It has been reported that the photocatalytic degradation of MB is a first-order reaction [50,51]. We can express the kinetics with the formula $\ln(C_0/C_t) = kt$, where k is the apparent rate constant. The k values obtained from the slopes of the $\ln(C_0/C_t)$ - t lines (Fig. 6(b)) are listed in Table 3. All of the correlation coefficients (R^2) were close to 1, indicating a good linear relationship of $\ln(C_0/C_t)$ - t . The photocatalytic MB degradation rate followed the sequence of $\text{BiVO}_{4-\delta}$ (0.0068 min^{-1}) < $\text{BiVO}_{4-\delta}\text{S}_{0.12}$ (0.0096 min^{-1}) < $\text{BiVO}_{4-\delta}\text{S}_{0.05}$ (0.0128 min^{-1}) < $\text{BiVO}_{4-\delta}\text{S}_{0.08}$ (0.0164 min^{-1}), which is the order in O_{ads} concentration and the reverse of the order in bandgap energy.

In order to study the effect of initial MB concentrations ($C_0 = 0.005, 0.01, 0.02, 0.03, \text{ and } 0.04 \text{ mmol/L}$), we measured the photocatalytic performance of $\text{BiVO}_{4-\delta}\text{S}_{0.08}$ for the degradation of MB under visible light illumination. The results are shown in Fig. 7. The photodegradation efficiency was enhanced with a decrease in initial MB concentration. This result was similar to that in the photodegradation of 2,4-dichlorophenoxyacetic acid over a Ca-Ce-W-TiO₂ composite catalyst under UV light irradiation [52]. With the decrease in initial MB concentration, the slope of the $\ln(C_0/C_t)$ - t line became steep, and the reaction rate was faster at a lower concentration (Fig. 7(b)). The k value (0.0052 min^{-1}) of the $\text{BiVO}_{4-\delta}\text{S}_{0.08}$ sample was much higher than that (0.0023 min^{-1}) of the $\text{Li}_9\text{Fe}_3(\text{P}_2\text{O}_7)_3(\text{PO}_4)_2$ sample for the photodegradation of MB in MB aqueous solution (0.03 mmol/L) under visible light illumination [53].

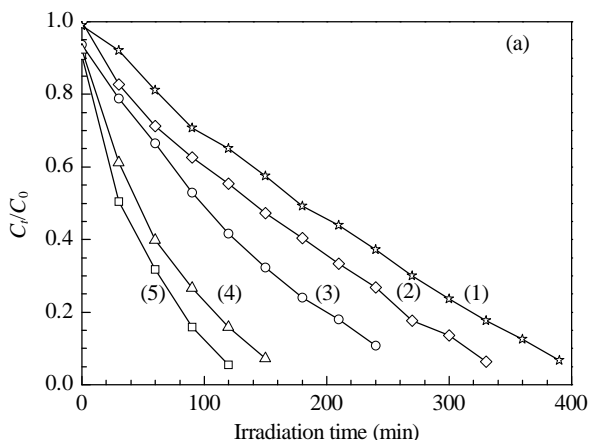


Fig. 7. Degradation of MB over 0.01 g of the $\text{BiVO}_{4-\delta}\text{S}_{0.08}$ sample at initial MB concentration of 0.04 (1), 0.03 (2), 0.02 (3), 0.01 (4), and 0.005 (5) mmol/L under visible-light ($\lambda \geq 400 \text{ nm}$) irradiation. Reaction conditions: temperature = 25°C , MB solution volume = 100 ml.

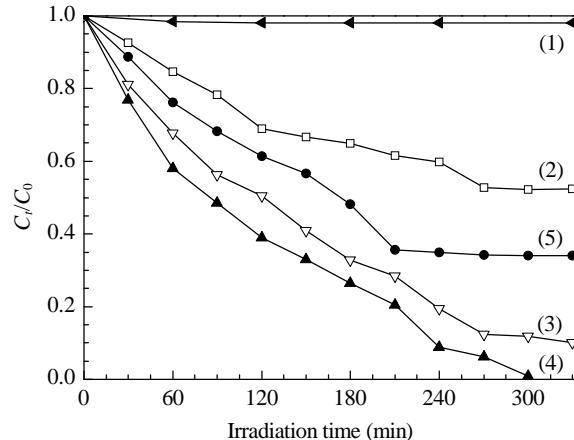
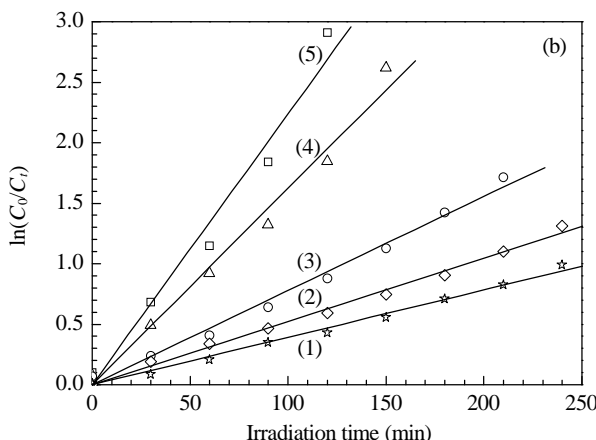


Fig. 8. Photocatalytic activities for the degradation of formaldehyde ($C_0 = 0.04\%$) in the absence (1) and presence of 0.1 g $\text{BiVO}_{4-\delta}$ (2), $\text{BiVO}_{4-\delta}\text{S}_{0.05}$ (3), $\text{BiVO}_{4-\delta}\text{S}_{0.08}$ (4), and $\text{BiVO}_{4-\delta}\text{S}_{0.12}$ (5) under visible light ($\lambda \geq 400 \text{ nm}$) illumination. Reaction conditions: temperature = 25°C , formaldehyde solution volume = 100 ml.

3.6. Photocatalytic degradation of formaldehyde

The photocatalytic degradation of formaldehyde over the samples in a 0.04% formaldehyde aqueous solution without the use of electron scavenger (e.g., H_2O_2 or Na_2S) was examined. For comparison, we also measured the direct photolysis of formaldehyde under visible light illumination. Figure 8 shows the photocatalytic performance of the samples for the degradation of formaldehyde. The formaldehyde concentration was almost unchanged in the direct photolysis process, indicating that the photolysis of formaldehyde was negligible under the adopted conditions. The formaldehyde conversion over the samples after 300 min reaction time increased in the order of $\text{BiVO}_{4-\delta}$ (48%) < $\text{BiVO}_{4-\delta}\text{S}_{0.12}$ (64%) < $\text{BiVO}_{4-\delta}\text{S}_{0.05}$ (90%) < $\text{BiVO}_{4-\delta}\text{S}_{0.08}$ (ca. 100%), in good agreement with the sequence of the photocatalytic performance for the degradation of MB. In their study of the photocatalytic decomposition of formaldehyde over a Pt-doped TiO₂ catalyst under UV light irradiation, Li et al. [54] observed that formaldehyde was totally decomposed within 80 min. Using $\text{V}_2\text{O}_5/\text{TiO}_2$ as the photocatalyst for



the degradation of formaldehyde, Akbarzadeh et al. [55] found that the degradation of formaldehyde under sunlight illumination was much better than that under visible or UV light irradiation.

It is generally accepted that photocatalytic performance is influenced by the crystal structure, crystallinity, particle morphology, surface area, oxygen vacancy, pore structure, and bandgap energy [5,56–59]. In the present work, the samples possessed several similar physical properties such as monoclinic scheelite crystal structure, porous architecture, and olive-like particle morphology. Although the $\text{BiVO}_{4-\delta}$ sample displayed the highest surface area ($12.5 \text{ m}^2/\text{g}$) and the strongest photon absorbing ability, it showed the worst photocatalytic activity for degradation of MB and formaldehyde. This result means that other factors that are more important determine the photocatalytic performance of the samples, e.g., the bandgap energy and surface oxygen vacancy (O_{ads}) concentration. The presence of $\text{Bi}^{5+}/\text{Bi}^{3+}$ and $\text{V}^{5+}/\text{V}^{4+}$ couples also contributed to the photocatalytic degradation of pollutants, with the $\text{Bi}^{5+}/\text{Bi}^{3+}$ and $\text{V}^{5+}/\text{V}^{4+}$ couples involved in the oxidization or reduction of toxic organic molecules through active species generated by the photo-generated electrons (e^-) and holes (h^+) on the photocatalyst surface. This reaction would be by the following equations:

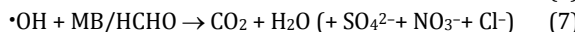
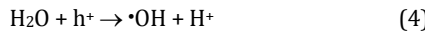
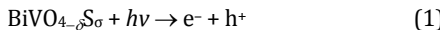


Photo-induced e^-/h^+ pairs are generated on the surface of the photocatalyst during irradiation (Eq. (1)). The photo-induced e^- can be easily trapped by Bi^{5+} and V^{5+} ions (Eqs. (2) and (3)), thus effectively reducing the recombination of e^-/h^+ pairs. The photo-induced h^+ oxidize H_2O molecules adsorbed on the photocatalyst surface into $\cdot\text{OH}$ and H^+ species (Eq. (4)), while the photo-induced e^- activate O_2 molecules adsorbed on the catalyst surface into O_2^- species (Eq. (5)), and H^+ reduce the active O_2^- species into $\cdot\text{OH}$ species (Eq. (6)). It is known that $\cdot\text{OH}$ species are the main active species in the photocatalytic reaction [60,61]. The organic molecules are oxidized by $\cdot\text{OH}$ species into inorganic molecules (Eq. (7)). Therefore, we think that active Bi^{5+} , V^{5+} , and O_{ads} species contribute to the direct or indirect generation of $\cdot\text{OH}$ species on the surface of the photocatalyst under visible light illumination, which promoted the photocatalytic degradation of MB and formaldehyde. In other words, doping S^{2-} into the $\text{BiVO}_{4-\delta}$ lattice improved photocatalytic activity due to the appearance of Bi^{5+} species and the increased amounts of V^{5+} and O_{ads} species. As shown in Figs. 6–8 and Table 3, the photocatalytic performance was enhanced greatly after the doping of sulfur into the $\text{BiVO}_{4-\delta}$ lattice. However, an excessive amount of sulfur doped was not beneficial for the enhancement in photocatalytic activity. Such a phenomenon was also observed by other researchers [49]. Although S-doping induced a decrease in photon absorbing ability, it increased the amount of surface active oxygen species. That is

to say, the doping of sulfur into the $\text{BiVO}_{4-\delta}$ lattice gave rise to an increase in O_{ads} concentration, thus enhancing photocatalytic activity. Therefore, it was concluded that the higher O_{ads} concentration and lower bandgap energy were the key factors that accounted for the excellent photocatalytic activity of the $\text{BiVO}_{4-\delta}\text{S}_{0.08}$ sample.

4. Conclusions

Porous $\text{BiVO}_{4-\delta}$ and S-doped samples $\text{BiVO}_{4-\delta}\text{S}_{0.05}$, $\text{BiVO}_{4-\delta}\text{S}_{0.08}$, and $\text{BiVO}_{4-\delta}\text{S}_{0.12}$ were prepared using the dodecylamine-assisted alcohol-hydrothermal method in the absence and presence of thiourea or Na_2S . All the samples had a single phase monoclinic crystal structure with surface areas of $8.4\text{--}12.5 \text{ m}^2/\text{g}$ and bandgap energies of $2.40\text{--}2.48 \text{ eV}$. Surface $\text{Bi}^{5+}/\text{Bi}^{3+}$ and $\text{V}^{5+}/\text{V}^{4+}$ couples were present on the S-doped samples. The highest O_{ads} species concentration was that on the $\text{BiVO}_{4-\delta}\text{S}_{0.08}$ surface. The amount of sulfur doped exerted a crucial effect on the photocatalytic performance of the sample. Under visible light illumination, the $\text{BiVO}_{4-\delta}\text{S}_{0.08}$ sample showed the best photocatalytic performance for the degradation of methylene blue and formaldehyde. A higher O_{ads} concentration and a lower bandgap energy were responsible for the excellent photocatalytic activity of $\text{BiVO}_{4-\delta}\text{S}_{0.08}$.

Acknowledgements

Chak Tong Au thanks Hong Kong Baptist University for financial support.

References

- Muktha B, Darriet J, Madras G, Row T N G. *J Solid State Chem*, 2006, 179: 3919
- Obregón Alfaro S, Martínez-de la Cruz A. *Appl Catal A*, 2010, 383: 128
- Ng Y H, Iwase A, Kudo A, Amal R. *J Phys Chem Lett*, 2010, 1: 2607
- Yin W Z, Wang W Z, Zhou L, Sun S M, Zhang L. *J Hazard Mater*, 2010, 173: 194
- Jiang H Y, Dai H X, Meng X, Ji K M, Zhang L, Deng J G. *Appl Catal B*, 2011, 105: 326
- Zhou Y, Vuille K, Heel A, Probst B, Kontic R, Patzke G R. *Appl Catal A*, 2011, 375: 140
- Naya S, Tanaka M, Kimura K, Tada H. *Langmuir*, 2011, 27: 10334
- Eda S, Fujishima M, Tada H. *Appl Catal B*, 2012, 125: 288
- Kohtani S, Koshiko M, Kudo A, Tokumura K, Ishigaki Y, Toriba A, Hayakawa K, Nakagaki R. *Appl Catal B*, 2003, 46: 573
- Tokunaga S, Kato H, Kudo A. *Chem Mater*, 2001, 13: 4626
- Zhang X, Ai Z H, Jia F L, Zhang L Z, Fan X X, Zou Z G. *Mater Chem Phys*, 2007, 103: 162
- Madhusudan P, Ran J R, Zhang J, Yu J G, Liu G. *Appl Catal B*, 2011, 110: 286
- Li Z H, Dong T T, Zhang Y F, Wu L, Li J Q, Wang X X, Fu X Z. *J Phys Chem C*, 2007, 111: 4727
- Li D, Ohashi N, Hishita S, Kolodiaznyi T, Haneda H. *J Solid State Chem*, 2005, 178: 3293
- Wang J S, Yin S, Zhang Q W, Saito F, Sato T. *J Mater Chem*, 2003, 13: 2348
- Li H X, Zhang X Y, Huo Y N, Zhu J. *Environ Sci Technol*, 2007, 41:

4410

- [17] Long R, English N J. *J Phys Chem C*, 2009, 113: 8373
- [18] Shen G Z, Cho J H, Yoo J K, Yi G-C, Lee C J. *J Phys Chem B*, 2005, 109: 5491
- [19] Jiang H Y, Meng X, Dai H X, Deng J G, Liu Y X, Zhang L, Zhao Z X, Zhang R Z. *J Hazard Mater*, 2012, 217–218: 92
- [20] Jiang H Y, Dai H X, Meng X, Zhang L, Deng J G, Liu Y X, Au C T. *J Environ Sci*, 2012, 24: 449
- [21] Meng X, Zhang L, Dai H X, Zhao Z X, Zhang R Z, Liu Y X. *Mater Chem Phys*, 2011, 125: 59
- [22] Liu Y X, Dai H X, Deng J G, Zhang L, Au C T. *Nanoscale*, 2012, 4: 2317
- [23] Jiang H Y, Dai H X, Meng X, Zhang L, Deng J G, Ji K M. *Chin J Catal* [蒋海燕, 戴洪兴, 孟雪, 张磊, 邓积光, 吉科猛. 催化学报], 2011, 32: 939
- [24] Zhou L, Wang W Z, Xu H L. *Cryst Growth Des*, 2008, 8: 728
- [25] Sun S M, Wang W Z, Zhou L, Xu H L. *Ind Eng Chem Res*, 2009, 48: 1735
- [26] Gregg S J, Sing K S W. *Adsorption, Surface Area and Porosity*. 2nd Ed. London: Academic Press, 1982. 61–84
- [27] Su J, Zou X-X, Li G-D, Wei X, Yan C, Wang Y-N, Zhao J, Zhou L-J, Chen J-S. *J Phys Chem C*, 2011, 115: 8064
- [28] Liu H M, Imanishi A, Nakamura R, Nakato Y. *Phys Stat Sol B*, 2008, 245: 1807
- [29] Li G S, Zhang D Q, Yu J C. *Chem Mater*, 2008, 20: 3983
- [30] Berglund S P, Flaherty D W, Hahn N T, Bard A J, Mullins C B. *J Phys Chem C*, 2011, 115: 3794
- [31] Ye H, Lee J, Jang J S, Bard A J. *J Phys Chem C*, 2010, 114: 13322
- [32] Dai H X, He H, Au C T. *Ind Eng Chem Res*, 2002, 41: 37
- [33] Hillebrecht F U, Fraxedas J, Ley L, Trodahl H J, Zaanen J, Braun W, Mast M, Petersen H, Schaible M, Bourne L C, Pinsukanjana P, Zettl A. *Phys Rev B*, 1989, 39: 236
- [34] Sada A, Eyman D P. *Ind Eng Chem Res*, 2011, 50: 9027
- [35] Chen Y S, Xie K, Liu Z X. *Appl Surf Sci*, 1998, 133: 221
- [36] Heber M, Grünert W. *J Phys Chem B*, 2000, 104: 5288
- [37] Zhu Y J, Sun Y Q, Niu X Y, Yuan F L, Fu H G. *Catal Lett*, 2010, 135:

152

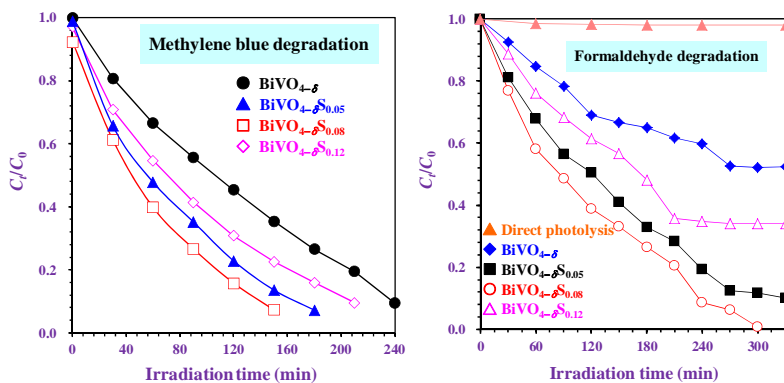
- [38] Machocki A, Ioannides T, Stasinska B, Gac W, Avgouropoulos G, Delimaris D, Grzegorczyk W, Pasiezna S. *J Catal*, 2004, 227: 282
- [39] Wei X-L, Fahlman M, Epstein A J. *Macromolecules*, 1999, 32: 3114
- [40] Ishida T, Choi N, Mizutani W, Tokumoto H, Kojima I, Azebara H, Hokari H, Akiba U, Fujihira M. *Langmuir*, 1999, 15: 6799
- [41] Liu Y, Ma J F, Liu Z S, Dai C H, Song Z W, Sun Y, Fang J R, Zhao J G. *Ceram Int*, 2010, 36: 2073
- [42] Ke D N, Peng T Y, Ma L, Cai P, Jiang P. *Appl Catal A*, 2008, 350: 111
- [43] Kudo A, Omori K, Kato H. *J Am Chem Soc*, 1999, 121: 11459
- [44] Jia Z F, Wang F M, Xin F, Zhang B Q. *Ind Eng Chem Res*, 2011, 50: 6688
- [45] Fu H B, Pan C S, Yao W Q, Zhu Y F. *J Phys Chem B*, 2005, 109: 22432
- [46] Zhou L, Wang W Z, Liu S W, Zhang L S, Xu H L, Zhu W. *J Mol Catal A*, 2006, 252: 120
- [47] Hussain S T, Khan K, Hussain R. *J Nat Gas Chem*, 2009, 18: 383
- [48] Yang K S, Dai Y, Huang B B. *J Phys Chem C*, 2007, 111: 18985
- [49] Izumi Y, Ito T, Peng S, Oka K, Shibata Y. *J Phys Chem C*, 2009, 113: 6706
- [50] Matos J, García A, Zhao L, Titirici M M. *Appl Catal A*, 2010, 390: 175
- [51] Syoufian A, Nakashima K. *J Colloid Interface Sci*, 2007, 313: 213
- [52] Akpan U G, Hameed B H. *Chem Eng J*, 2011, 173: 369
- [53] Ji F, Li C L, Zhang J H. *ACS Appl Mater Interfaces*, 2010, 2: 1674
- [54] Li Y X, Lu G X, Li S B. *Chemosphere*, 2003, 52: 843
- [55] Akbarzadeh R, Umbarkar S B, Sonawane R S, Takle S, Dongare M K. *Appl Catal A*, 2010, 374: 103
- [56] Amano F, Nogami K, Ohtani B. *J Phys Chem C*, 2009, 113: 1536
- [57] Pan H, Gu B H, Zhang Z Y. *J Chem Theory Comput*, 2009, 5: 3074
- [58] Hwang D W, Cha K Y, Kim J, Kim H G, Bae S W, Lee J S. *Ind Eng Chem Res*, 2003, 42: 1184
- [59] Yan T J, Long J L, Shi X C, Wang D H, Li Z H, Wang X X. *Environ Sci Technol*, 2010, 44: 1380
- [60] Sun J H, Yang H, Xian T, Wang W P, Feng W J. *Chin J Catal* [孙军辉, 杨华, 县涛, 王伟鹏, 冯旺军. 催化学报], 2012, 33: 1982
- [61] Xiang Q J, Yu J G, Wong P K. *J Colloid Interface Sci*, 2011, 357: 163

Graphical Abstract

Chin. J. Catal., 2013, 34: 1617–1626 doi: 10.1016/S1872-2067(12)60632-9

Effect of sulfur doping on the photocatalytic performance of BiVO₄ under visible light illumination

Zhenxuan Zhao, Hongxing Dai*, Jiguang Deng, Yuxi Liu, Chak Tong Au*
Beijing University of Technology; Hong Kong Baptist University



Porous BiVO₄- δ and BiVO₄- δ -S σ are fabricated using dodecylamine-assisted alcohol-hydrothermal strategy. The higher O_{ads} concentration and lower bandgap energy account for excellent photocatalytic performance of BiVO₄- δ -S_{0.08} for methylene blue and formaldehyde degradation.

硫掺杂橄榄状BiVO₄上可见光降解亚甲基蓝和甲醛水溶液性能

赵振璇^a, 戴洪兴^{a,*}, 邓积光^a, 刘雨溪^a, 区泽棠^{b,#}

^a北京工业大学环境与能源工程学院化学化工系催化化学与纳米科学实验室, 北京100124

^b香港浸会大学理学院化学系, 香港

摘要: 在无和有S源(Na₂S或硫脲)存在的条件下, 采用十二胺辅助的醇-水热法制备了多孔单斜晶相结构的BiVO_{4-δ}和不同含量S掺杂的BiVO_{4-δ}光催化剂。利用多种手段表征了催化材料的物化性质, 评价了它们在可见光照射下催化降解亚甲基蓝或甲醛的反应活性。结果表明, 所制光催化剂为单斜白钨矿晶相结构, 具有多孔橄榄形状貌, 比表面积为8.4–12.5 m²/g, 带隙能为2.40–2.48 eV。在S掺杂BiVO_{4-δ}表面同时含有Bi⁵⁺, Bi⁴⁺, V⁵⁺和V⁴⁺物种。S掺杂对BiVO_{4-δ}光催化剂的活性影响很大。在可见光下照射下, BiVO_{4-δ}S_{0.08}光催化剂对亚甲基蓝和甲醛降解反应显示出最高的光催化活性, 这与其较高的表面氧物种浓度和较低的带隙能相关。

关键词: 硫掺杂; 钒酸铋; 可见光催化; 橄榄形状貌; 亚甲基蓝降解; 甲醛水溶液降解

收稿日期: 2013-03-11. 接受日期: 2013-06-05. 出版日期: 2013-08-20.

*通讯联系人. 电话: (010)67396118; 传真: (010)67391983; 电子信箱: hxdai@bjut.edu.cn

#通讯联系人. 电话: (852)3411-7067; 传真: (852)3411-7348; 电子信箱: pctau@hkbu.edu.hk

基金来源: 国家自然科学基金(21077007); 学科与研究生教育基金(005000541212014); 北京市教委创新团队项目(PHR201107104); 香港浸会大学基金(FRG2/09-10/023)。

本文的英文电子版由Elsevier出版社在ScienceDirect上出版(<http://www.sciencedirect.com/science/journal/18722067>)。